Magnetoelastic Properties of Superconducting Niobium†

G. W. Goodrich and J. N. Lange
Department of Physics, Oklahoma State University, Stillwater, Oklahoma 74074
(Received 2 August 1971)

Changes in elasticity as a result of the superconducting transition are observed in high-purity niobium. The stiffness changes in niobium are quite anisotropic and dependent on the acoustic mode, suggesting a microscopic mechanism which is dependent on the crystalline symmetry, perhaps through the band structure. Imperfections and impurities have little effect on the stiffness changes. A residual stiffness resulting from trapped vortices is used to calculate the forces binding the vortices to imperfections. The magnitudes of the binding forces suggest a stronger binding mechanism than provided by elastic gradients and might be associated with a dynamic interaction between the vortex and the motion of dislocations. The attenuation of the acoustic wave is observed to decrease upon entering the mixed state and finally to increase rapidly to its normal-state value at the second critical field (H_{c2}). The decrease in attenuation is interpreted as being due to the pinning of free dislocation segments by vortices, which leads to a mismatch between the acoustic wave and the dislocation system and a resulting decrease in the energy absorbed from the acoustic wave. At fields immediately above H_{c2}, small changes in attenuation are observed which may be attributed to the presence of fluctuating Cooper pairs. The second critical field is observed to increase with increases in dislocation density without any accompanying increase in the normal-state resistance. This change is used to calculate a parameter proportional to the phonon mean free path which modifies the coherence length in a manner similar to the electron mean free path. The magnitudes of this parameter are comparable to the average dislocation separations, suggesting that the coherence of the Cooper pairs is limited by scattering from dislocations.

I. INTRODUCTION

Transition to the superconducting state leads to changes in the elastic properties of a solid. These elastic changes are used to study the behavior of the mixed state in niobium as well as to provide information on the microscopic mechanism associated with the changes in lattice properties due to the superconducting transition. Both the stiffness[1,2] and the acoustic attenuation[3] are less in the superconducting state than in the normal state. The decrease is a few parts per million (ppm) for the former while often orders of magnitude for the latter. Of particular interest in this investigation are the magnitude and magnetic field dependence of the elastic changes at fixed temperatures for niobium.

The decrease in the acoustic attenuation due to the onset of the superconducting state has its origin in the change in excitation spectrum of the charge carriers. The magnitude of the attenuation change can be accounted for at high frequencies and low temperatures ($T < T_C$) as being due to the lack of available excited states for the charge carriers interacting with the lattice (at least for phonons with energies less than twice the superconducting gap energy). The superconductor in the Meissner state then exhibits acoustic behavior characteristic of insulators.[4] At low acoustic frequencies the attenuation has quite a different origin. The contribution of the electron-lattice interaction of the Pippard type[5] to the normal-state attenuation can be quite small and most of the attenuation has its origin in the motion of imperfections such as dislocations. In this investigation, the electron-lattice attenuation is always less than 5% of the observed attenuation. The low-frequency attenuation due to the superconducting transition considered in this investigation is, therefore, almost exclusively due to the change in dynamics of *imperfections such as dislocations*. The motion of the imperfections is affected by the onset of superconductivity through the change in viscous damping by the normal electons. The superconducting transition affects the dynamics of the dislocation by changing the viscous damping of its motion from overdamped in the normal state to underdamped in the Meissner state.

The change in stiffness induced by the superconducting transition results from modification of the lattice interaction by the pair state. An empirical investigation of the magnitude of the stiffness change due to the superconducting transition reveals no appreciable effect by factors such as dislocation and impurity density which are effective in changing the stiffness of the normal state. The stiffness change due to the superconducting transition is quite anisotropic and appears to be dependent on either the band structure or the details of the atomic potentials. This result is conceptually similar to the deformation-potential inter-

action invoked to explain elastic changes in semiconductors when charge carriers are added.

The field dependence of the vortex size and density is obtained for the mixed state of niobium using a model of the vortex and its interaction. The field dependence of the vortex density does not change appreciably as a function of dislocation density and impurities. A residual stiffness resulting from trapped flux remains after cycling the external magnetic field above the second critical field (H_{c2}). Using the vortex interaction model of de Gennes and the phenomenological model for the vortex density, the binding force per unit length can be calculated without an *a priori* model of the vortex-lattice interaction. The magnitude of the binding force and behavior as a function of dislocation and impurity density suggests that the vortex trapping is not due to binding to dislocations by elastic gradients but rather may involve a dynamic interaction between the vortex and a local electromagnetic field resulting from the vibration of the free dislocation segments.

Attenuation of the acoustic wave in the mixed state reflects the excitation spectrum[6] of the charge carriers as well as a contribution due to lattice imperfections such as dislocations.[7,8] The dislocation attenuation is large compared to the purely electronic contribution in both the superconducting and the normal states at the low frequencies used in this investigation. The contribution of the dislocation motion to the total attenuation depends on the matching conditions between the frequency of the acoustic wave and the resonant frequencies of the distribution of free dislocation segments in the stretched-string dislocation model. Some of the features of the field dependence of the attenuation at low fields are explained in terms of the changing coupling between the acoustic wave and the dislocation motion. In particular, an initial decrease in attenuation as the flux penetrates the bulk of the specimen appears to be caused by an alteration of these matching conditions due to the pinning of the dislocation motion by vortices. At fields approaching the second critical field, the field dependence of the attenuation is dominated by the normal electronic component returning to damp the dislocation motion.

The coherence of the Cooper pairs is modified not only by the scattering centers that limit the electron mean free path[7] but also by those which limit the phonon mean free path. This second limitation is observed as an increase in the second critical field with increased imperfection concentration without an accompanying increase in the low-temperature resistivity. Using a solution to the linearized form of the Landau-Ginsburg equation, the coherence length modified by imperfection scattering can be calculated. The magnitude of the imperfection limitation is similar to the separation of free dislocation segments expected in annealed high-purity metals. This suggests that the motion of the dislocation segments is effective in limiting the coherence of the Cooper pairs.

II. EXPERIMENTAL ARRANGEMENT AND RESULTS

The elastic changes due to the superconducting state are determined from the resonance frequency and decay time of a rod of niobium ($\frac{1}{4}$-in. diam). These observations are used to calculate the change in stiffness (modulus) and attenuation (loss factor).[9] By careful mounting and dislocation from the electronic drive system, very low acoustic losses are observed with a resulting resolution of $\frac{1}{10}$ ppm in the stiffness.[10] All measurements are at a fixed temperature, with the stiffness and attenuation being monitored simultaneously. The resonance frequency of the fundamental longitudinal mode is in the 40–50-kHz range while the torsional-mode frequency is in the 20–30-kHz range. Through the use of a unique capacitive drive and detection system,[11] either the longitudinal or the torsional mode can be excited for a given specimen without changing the experimental arrangement. This facilitates a comparison of the elastic changes between the two modes without introducing complications due to changes in mounting, drive systems, or aging.

The specimens are in the form of rods with the external magnetic field applied perpendicular to the axis. For the mixed state, this leads to a demagnetization factor of approximately one-half. The axial orientations of the single-crystal rods are pure-mode directions for longitudinal waves so that the energy of the mode propagates in the same direction as the wave vector. For the cubic symmetry of the niobium this corresponds to the [100], [110], and [111] directions. The torsional wave is a pure mode when propagating in directions for which the transverse modes are cylindrically degenerate. For cubic symmetry, these are the [100] and [111] directions.

The capacitive drive excites modes with a constant distribution over the cross section. The form of the elastic equations most amenable[12] to these boundary conditions is expressed in terms of the compliance components S_{ij}. The stiffness moduli (Σ_k^m) are equal to the reciprocal of the compliance elements and are labeled with a subscript indicating the direction of propagation and a superscript indicating the mode type (c for compressional mode and t for torsional mode). A summary of the stiffness moduli in terms of the compliance elements and stiffness constants is given in Table I for the various modes used in this investigation.

The electronic characteristics of the specimens are listed in Table II. The residual resistance ratio (RRR) is calculated using an extrapolated

TABLE I. Stiffness moduli for compressional and torsional modes propagating along high-symmetry directions in crystals of cubic symmetry.

Wave vector (axial orientation)	Displacement	Mode	Compliant element	Stiffness moduli	Stiffness constants
[100]	[100]	compressional	S_{11}	Σ^C_{100}	$\frac{C_{11}+C_{12}}{(C_{11}-C_{12})(C_{11}+2C_{12})}$
[100]	⟨100⟩	torsional	S_{44}	Σ^T_{100}	C_{44}
[111]	[111]	compressional	$\frac{1}{3}(S_{11}+2S_{12}+4S_{44})$	Σ^C_{111}	$\frac{C_{44}+4(C_{11}+2C_{12})}{3C_{44}(C_{11}+2C_{12})}$
[111]	⟨111⟩	torsional	$\frac{1}{3}(S_{11}-S_{12}+S_{44})$	Σ^T_{111}	$\frac{C_{44}+3(C_{11}-C_{12})}{3C_{44}(C_{11}-C_{12})}$
[110]	[110]	compressional	$\frac{1}{2}(S_{11}+S_{12}+2S_{44})$	Σ^C_{110}	$\frac{C_{11}C_{44}+2(C_{11}-C_{12})(C_{11}+2C_{12})}{2C_{44}(C_{11}-C_{12})(C_{11}+2C_{12})}$

value of the magnetoresistance. The magnetic field used to quench the superconducting state is applied in a plane perpendicular to the direction indicated by the axial orientation. The measurements in Table II are for specimens in an annealed state. The critical fields are determined from the magnetic field dependence of the elasticity. Dislocation densities in the high-purity annealed specimens[13] (Nos. 4 and 5) are in the range 10^4–10^5 cm^{-2} based on observations made on similarly prepared specimens from the same laboratory.[14] Mechanical damage is introduced by both quenching and deformation. The quenching occurs in silicon oil from 1000 °C to room temperature in approximately 20 sec. The deformations are produced along the radius of the rod in a symmetric fashion to preserve the circular cross section.

All measurements are made at a fixed temperature in a magnetic field perpendicular to the axis of the rod. Thermal contact to a liquid-helium bath is through an ambient of 500 mTorr of helium gas. No time-dependent changes are observed, which suggests significant Joule heating from the acoustic energy or eddy currents due to the vibration motion in the magnetic field. The strain amplitudes of the acoustic wave are estimated at 10^{-8} m/m.

The specimens are etched before each run to remove surface damage, resulting in a highly reflective surface. The measurement procedure involves cooling the specimen below the superconducting critical temperature before applying a magnetic field. Measurements through the Meissner state and into the mixed state are made without any trapped flux. The field is cycled well above H_{c2} to obtain the normal-state field dependence of the elasticity for that particular sample and acoustic mode. The stiffness and attenuation are also monitored in the decreasing field to determine the hysteresis due to trapped flux.

The changes in the elastic properties as a function of field are calculated as fractional changes normalized to the superconducting-state value. For example, the fractional change in stiffness as seen by a torsional mode propagating along the [100] direction is given by

$$\frac{\Delta\Sigma^T_{100}}{\Sigma^T_{100}} = \frac{\Sigma^T_{100}(H) - \Sigma^T_{100}(S)}{\Sigma^T_{100}(S)} \quad , \tag{1}$$

where $\Sigma^T_{100}(S)$ is the stiffness in the Meissner state and $\Sigma^T_{100}(H)$ is the field-dependent stiffness. The fractional change in stiffness exhibits no change in the Meissner state for a virgin sample, as can be seen in Fig. 1. As the flux begins to penetrate at a field of $\frac{1}{2} H_{c1}$ the fractional change in stiffness increases to the normal-state value at H_{c2}. Further increases in field lead to a quadratic stiffness increase expected in the normal state.[15] The total change in the fractional stiffness is obtained by subtracting from the value at H_{c2} the normal-state quadratic field dependence.[16] As the field is decreased below H_{c2} to zero external field, a hysteresis in the stiffness results from trapped vortices.

TABLE II. Residual resistance ratio (RRR) and axial orientation for annealed niobium single-crystal rods. The critical fields are determined from the magnetic field dependence of the stiffness.

Sample No.	Axial orientation	RRR	ρ(4.2 °K) ($\mu\Omega$ cm)	H_{c1} (kOe)	H_{c2} (kOe)
1	[100]	30	0.64	1.30	3.20
2	[110]	86	0.17	1.40	2.90
3	[111]	55	0.34	1.44	3.00
4	[100]	2500	6.8×10^{-3}	1.60	2.65
5	[111]	2500	7.5×10^{-3}	1.70	2.70

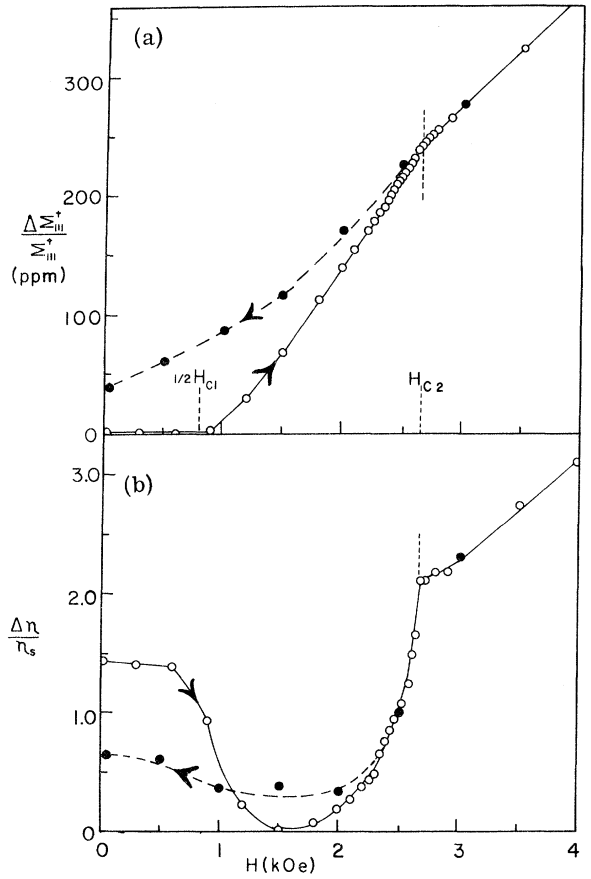

FIG. 1. (a) Fractional change in stiffness as a function of magnetic field for a torsional mode propagating along the [111] direction in a high-purity niobium single crystal (No. 5). Cooling to obtain the superconducting state is done in the absence of an external magnetic field. No change in stiffness is noted as the field is increased (○) until the mixed state is established at $\frac{1}{2}H_{c1}$ (demagnetization factor of $\frac{1}{2}$ for the external field perpendicular to the rod axis). The critical fields are obtained from the changes in slope of the fractional change in stiffness. The total stiffness change due to the superconducting transition is obtained by subtracting the normal-state field-dependent stiffness from the observed value at H_{c2}. As the field is decreased (●) the stiffness exhibits a hysteresis due to trapped flux. The residual stiffness in zero external field is due to vortices trapped by imperfections; $T=4.2$ °K. (b) Fractional change in attenuation as a function of magnetic field for a torsional mode propagating along the [111] axis in specimen No. 5. The decrease in attenuation begins at $\frac{1}{2}H_{c1}$ in increasing fields (○) as the flux begins to penetrate the bulk. The normal-state fractional change ($H>H_{c2}$) is quadratic with field. The attenuation exhibits a hysteresis in decreasing fields (●) due to trapped vortices. This is less when the trapped vortices are present than in the Meissner state; $T=4.2$ °K.

If the temperature of the material is raised above T_c this residual stiffness disappears and its previous value in the Meissner state is reobtained.

The magnitude of the stiffness increase in the normal state of the high-purity niobium is more complex than has been observed previously. The normal-state longitudinal stiffness for propagation along the [111] axis exhibits an anisotropy which varies with the direction of the field relative to the crystalline axes while maintaining a constant angle with respect to the direction of propagation. Longitudinal propagation along the [100] axis exhibits no such anisotropy when the field is rotated in the ⟨100⟩ plane. These effects appear to be associated with the anisotropic magnetoresistive tensor and will be considered in detail elsewhere. The torsional mode exhibits similar anisotropies but the magnitudes are dependent on the imperfection concentration, in contrast to the longitudinal mode. The anisotropy disappears in the severely deformed material and the torsional stiffness changes increase by a factor of 100 (at 3 kOe) over that observed in the annealed crystal. The stiffness changes of the torsional mode appear to be dominated by dislocation behavior[11] rather than by free-electron dynamics in the magnetic field, while the longitudinal mode exhibits what appears to be magnetoresistive effects.

The fractional change in attenuation as a function of field exhibits more complex behavior, as can be seen in Fig. 1(b). Initially the attenuation decreases as the flux penetrates the bulk with the fractional change becoming negative. This decrease is not observed for low-purity material or in high-purity material with a large imperfection concentration. As the magnetic field increases and approaches H_{c2} the attenuation increases rapidly to the normal-state value. The size of the increase is dependent on the type of acoustic mode and the propagation direction. As the field is decreased below H_{c2} a hysteresis due to trapped vortices is also observed in the attenuation such that at zero external field the attenuation is lower than in the virgin Meissner state. Much of the low-field behavior of the attenuation is interpreted in terms of the interaction of dislocations with the vortices.

In the following an idealized model of dislocations will be assumed. The dislocation line will have a characteristic average length which is pinned intermittantly by impurities or other dislocations to form segments. These segments are free to vibrate between the pinning points in a manner analogous to a stretched string as proposed by Koehler[17] and Granato and Lucke[18] (KGL). The length of the string determines in part the resonance frequency of oscillation. The degree of excitation of the free segment by the acoustic wave is determined by the shear stress in the plane of the string and the relative frequencies of the acoustic mode and the resonance of the free segment. The total energy absorbed by the dislocation is then deter-

TABLE III. Fractional change in the stiffness moduli in ppm as a result of transition from the superconducting to the normal state at $T=4.2$ °K. The normal-state field dependence has been subtracted.

Sample No.	RRR	$\frac{\Delta\Sigma^C_{100}}{\Sigma^C_{100}}$	$\frac{\Delta\Sigma^T_{100}}{\Sigma^T_{100}}$	$\frac{\Delta\Sigma^C_{111}}{\Sigma^C_{111}}$	$\frac{\Delta\Sigma^T_{111}}{\Sigma^T_{111}}$
1	30	65	193		
4	2500	25	234		
3	55			203	211
5	2500			215	130

mined by the polarization of the acoustic mode, th free-segment length and stiffness (resonance frequency), the damping, and the density of dislocations. The dislocation damping varies from overdamped in the normal state, due to viscous electron reaction to its motion, to underdamped in the superconducting state.

III. STIFFNESS

Transition to the superconducting state results in a decrease in the stiffness of a solid. The specific interaction leading to the stiffness change has not been isolated. It appears to involve changes in the electronic excitation spectrum due to the formation of Cooper pairs as well as their interaction with the harmonic components of the ionic potential. The change in stiffness in niobium is observed to be quite anisotropic, depending on both the crystalline direction of propagation and the specific lattice deformation. The total fractional change in stiffness is observed to vary by a factor of 10 (Table III) for different propagation directions and displacement polarizations in single crystals with nearly the same impurity concentration and thermal history. The longitudinal mode propagating along the [100] direction exhibited the smallest fractional change in velocity while the transverse mode along this same direction exhibited the largest change.

Changes in the RRR by a factor of 100 lead to only small alterations in the total fractional change in stiffness. For some directions and polarizations the fractional change increases while for others it decreases with increasing purity. The longitudinal-mode fractional change in stiffness along the [100] direction decreases by a factor of 2.6 with the increase in impurity while the transverse stiffness along the same direction increases by 20%. The impurity dependence of the stiffness changes caused by the superconducting transition is dominated by the elastic anistropy and does not lead to any universal pattern for superconducting stiffness changes in niobium single crystals. The samples considered in Table II are in the clean limit for which the electronic mean free path (l_e) is larger than the intrinsic coherence length (ξ_0) and thus may be dominated by the symmetry of the electronic and lattice structure rather than the impurity distribution.

The introduction of mechanical damage by quenching and deformation is even less effective than small impurity changes in modifying the fractional change in stiffness due to the superconducting transition. The normal-state stiffness decreased small amounts (typically 2% for the longitudinal stiffness and 4.5% for the transverse stiffness) as a result of an increase in an initially low dislocation density. The fractional change in stiffness due to the superconducting transition, however, is unaffected (Table IV) by mechanical damage, indicating that the contribution of dislocation motion to the stiffness of the solid is the same in the superconducting and normal states. The change in dislocation parameters in the superconducting state has a considerably more significant effect on the acoustic attenuation than on the stiffness and will be considered in a subsequent section.

The stiffness changes due to the superconducting transition appear to result from an interaction which is not changed radically by impurities and not at all by imperfections. The significant anisotropy and mode dependence of the fractional change in stiffness suggest a microscopic process which is related to the symmetry of the harmonic components of the lattice interactions and the band structure. Effects due to the overlapping s and d bands of niobium[19] have been invoked to explain[20] the behavior of the thermal conductivity of niobium[21] in the superconducting state. The symmetry of the band structure might well play a role in the change in stiffness because of the anistropy of the density of states of the d orbitals.

The stiffness of semiconductors is observed to change with charge carrier density in a manner which is dependent on the symmetry of the band structure.[22,23] The phenomenological description of the stiffness changes in semiconductors may

TABLE IV. Dependence of the total change in stiffness due to the superconducting transition on the mechanical damage for the high-purity (RRR-2500) niobium single crystals; $T=4.2$ °K.

Sample		$\frac{\Delta\Sigma^C_{100}}{\Sigma^C_{100}}$	$\frac{\Delta\Sigma^C_{111}}{\Sigma^C_{111}}$	$\frac{\Delta\Sigma^T_{100}}{\Sigma^T_{100}}$	$\frac{\Delta\Sigma^T_{111}}{\Sigma^T_{111}}$
No. 4 [100]	annealed	25		234	
	quenched	28			
	5% deformation	26			
No. 5 [111]	annealed		215		130
	quenched				130
	0.3% deformation				129

also be applicable to superconductors. The stiffness in the semiconductors is observed to change proportionally to the specific deformation potential associated with the lattice distortion[24,25] and the density of states at the Fermi energy for directions affected by the lattice distortion. By analogy to the behavior of semiconductors, the stiffness of a superconductor may be viewed as changing due to the formation of the Cooper pairs and the change in nature of the density of states. The deformation potential of the semiconductor is not altered appreciably when charge carriers are added through doping, but it is unlikely that similar behavior will be exhibited by a metal which undergoes a superconducting transition. Since the deformation potential represents an effective force to preserve charge neutrality, its alteration is plausible when pairing occurs since the interaction has a coherence over many atomic units and is long range on the scale of the deformation potential of the normal state. Although the deformation-potential approach seems more complex in calculating the stiffness changes in superconductors than in semiconductors, it appears useful to pursue it for lack of an apparent alternative.

IV. VORTEX PINNING

Hystersis in the magnetic field dependence of the transport properties of type-II superconductors results from trapped flux. The presence of trapped vortices has been envisioned by Essmann and Trauble[26] with electron microscopy of powder patterns. Elastic properties of type-II superconductors also exhibit a hysteresis in the form of an increased stiffness and attenuation after cycling above H_{c2}. The stiffness is particularly useful in investigating aspects of the flux pinning since it can be directly related to the density and separation of the vortices using an established model of the current vortex.

The fractional change in the longitudinal stiffness ($\Delta L/L$) has been shown to be directly proportional to the normal volume fraction in the mixed state through simultaneous observation of the magnetic susceptibility and the field dependence of the stiffness.[27] The field dependence of the fractional change in stiffness can be written in terms of the number of vortices per unit surface $[n(H)]$ times the area of the normal core of the vortex. Assumming a model of the vortex with a normal core of a radius equal to the coherence length (ξ), the area of the core can be computed.[28] The fractional change in longitudinal stiffness becomes

$$\frac{\Delta L}{L} = \left(\frac{L_N - L_S}{L_S}\right) \pi \xi^2 n(H), \tag{2}$$

where L_N is the normal-state stiffness and L_S is the stiffness of a virgin specimen in the Meissner state. The factor in parentheses is simply the total change in stiffness between the virgin normal and superconducting states whose values are tabulated in Sec. III. When the field is decreased from above H_{c2}, the flux trapped in the bulk of the specimen leads to a residual stiffness. This residual stiffness is given by

$$\left(\frac{\Delta L}{L}\right)_R = \left(\frac{\Delta L}{L}\right)_T n_R \pi \xi^2 \quad , \tag{3}$$

where n_R is the residual vortex density. The number of vortices per unit area can be calculated from the observed total change in stiffness and residual stiffness as

$$n_R = \left[\left(\frac{\Delta L}{L}\right)_R \Big/ \left(\frac{\Delta L}{L}\right)_T\right] \frac{1}{\pi \xi_0^2} \ , \tag{4}$$

using empirical values of the coherence length obtained from other sources. The average separation of the trapped vortices is then proportional to the reciprocal of the surface density. The average separation of the vortices calculated from the stiffness is comparable to the values observed directly by Essmann and Trauble.

To simplify identification of bulk-trapping mechanisms, the surface of the specimen is strongly etched as a precursor to each experiment, minimizing the effect of surface damage on the flux pinning. A series of measurements of the residual stiffness after successive severe etchings yielded identical results indicating that the flux pinning due to surface damage is not a significant contribution to the total residual stiffness for the etched specimens. The trapped flux is assumed to be pinned by a bulk phenomenon.

As illustrated in Table V, the trapped vortex density calculated from Eq. (4) is relatively insensitive to the impurity concentration. In fact, an increase in the RRR of a factor of 45 leads to an increase in the residual vortex density by only a factor of 3. The impurities themselves do not appear to be effective in trapping vortices, at least in the clean limit ($l_e > \xi_0$).

The major responsibility for flux pinning appears to be bulk imperfections and dislocations in particular. The observed trapped vortex does increase when the specimen is severely deformed (5% length

TABLE V. Trapped vortex density (n) resulting from cycling the external magnetic field above H_{c2}. The result is calculated from the longitudinal residual stiffness using Eq. (4); $T = 4.2$ °K.

Sample No.	RRR	n (10^9 cm^{-2})	Field direction
3	55	1.11	⟨111⟩
5	2500	3.65	⟨111⟩

TABLE VI. Effect of imperfections on the trapped vortex density in sample No. 4 using the longitudinal-mode residual stiffness and Eq. (4); $T = 4.2$ °K.

Condition	n (10^9 cm^{-2})
annealed	4.30
quenched	2.69
deformed	5.78

change), as seen in Table VI. The effectiveness of the trapping is dependent on the details of the dislocation distribution such as the average length and density. This is reflected in the different effects of quenching and deformation exhibited in Table VI. When the specimen is quenched, dislocation loops of shorter average lenghts result and the trapped vortex density decreases. It would appear that the relative size of the dislocation and the vortex affect the degree of pinning. When the vortex encounters a dislocation line or loop (D) smaller than its dimensions ($D > 2\xi$) the effective interaction is reduced. This is consistent with the lack of pinning of vortices to isolated impurities. Long dislocation lengths or higher densities increase the number of trapped vortices due to the increased pinning force.

An estimate of the pinning force per unit length of the vortex can be obtained by assuming the lattice pinning force balances the repulsive electromagnetic vortex interactions. For a homogeneous distribution of vortices the repulsive force per unit length for vortices on the exterior of the distribution can be calculated using an expression derived by de Gennes[29] and given by

$$f = (\phi_0^2/8\pi^2\lambda^3)e^{-r/\lambda} \quad , \tag{5}$$

where ϕ_0 is the quantized flux filament (2×10^{-7} G cm^2), λ is the London penetration depth, and r is the distance between the vortices. This repulsive force acts on vortices not symmetrically surrounded by neighbors and must be countered by the pinning force to obtain an equilibrium of pinned vortices at zero field. The magnitudes of the repulsive force per unit length are given in Table VII for separations derived from the residual vortex densities. This result does not depend on any specific pinning mechanism but only on the electromagnetic interactions of the vortices.

TABLE VII. Electromagnetic repulsive force between trapped vortices calculated from Eq. (5) and the vortex densities of Tables V and VI; $T = 4.2$ °K. The specimens are in an annealed state.

Specimen No.	RRR	Force (dyn cm^{-1})
3	55	0.075
4	2500	1.51
5	2500	0.92

A specific mechanism for the pinning of vortices is the interaction of the elastic gradients of the dislocations with the elastic gradient established between the normal core and superconducting exterior of the vortex. The binding force on the vortex due to this mechanism was calculated by Webb[30] for different vortex and dislocation orientations and ranged from 10^{-3} dyn cm^{-1} for vortices along the dislocation to 10^{-4} dyn cm^{-1} for other orientations. These values are considerably below those calculated from the repulsive electromagnetic interaction of the vortices. The elastic-gradient coupling is far weaker than necessary to balance the electromagnetic repulsion of the vortices, which may be balanced by a dynamic coupling of the vortex with the local electromagnetic fields generated by vibration of the free dislocation segment.

V. ATTENUATION

The attenuation of the acoustic wave in a superconductor in the mixed state results from a complexity of interactions involving the charge carrier excitation spectrum and the lattice. Particularly significant at the low frequencies used in this investigation is the contribution of lattice imperfections such as dislocations. The attenuation of the wave due to electron dynamics is less than 5% of the observed value. The effects of the dislocations and impurities on the attenaution do not appear to be independent in either the normal state[31] or the Meissner state.[32] This is illustrated in Table VIII for the normal state. The torsional-mode attenuation is seen to increase with increasing imperfec-

TABLE VIII. Loss factors for the longitudinal and torsional modes in niobium in the normal state. An external magnetic field of 3 kOe is applied; $T = 4.2$ °K.

Sample	Condition	Longitudinal η (10^{-6} Np)	Torsional η (10^{-6} Np)
No. 3 [111] RRR=55	annealed	17.2	1.40
	quenched		1.87
	deformed		19.4
No. 5 [111] RRR=2500	annealed	16.2	12.6
	quenched		9.90
	deformed		6.58
No. 4 [100] RRR=2500	annealed	5.18	27.7
	quenched	5.43	
	deformed	3.66	

tion concentration in the low-purity material (No. 3) while decreasing in the high-purity material (No. 5) of the same orientation. Along a different direction in the high-purity material, the longitudinal attenuation also decreases with increasing imperfection concentration.

In the Meissner state the attenuation is again dependent on the imperfection and impurity concentration (Table IX). The torsional-mode attenuation in the low-purity material increases with increasing imperfection concentration while decreasing in the high-purity material, as is observed in the normal state. The longitudinal attenuation is anomalous as it increases in the Meissner state with increasing imperfection changes while decreasing in the normal state.

This rather complex behavior of the attenuation as a function of imperfection distribution appears to be related to the interaction of the impurities and the dislocation motion which in turn affect the coupling of the acoustic mode to the dislocation system. The amplitude dependence of the attenuation in the low-purity specimen decreases as the imperfection concentration increases indicating an increased pinning by other dislocations rather than impurities. No appreciable amplitude dependence of the attenuation is observed in the high-purity material. The pinning mechanism is important in determining the excitation range of the dislocation system and the ultimate effect on the matching conditions with the acoustic wave. As the damage is increased for an initially annealed high-purity single crystal, the dislocations become so numerous that they begin to pin themselves. The resulting change in length of the free segments shifts their resonance frequency to higher values. The matching between the fixed-frequency acoustic wave and the vibrating dislocation line degrades as a result of the detuning and less of the acoustic energy is absorbed by the dislocation system. The environment of the dislocation is quite different in the Meissner state compared to the normal state. In the Meissner state the motion of the dislocation is underdamped while in the normal state the electronic viscosity overdamps the motion. This may, in part, be the origin of the difference in imperfection dependence of the longitudinal and torsional modes in the high-purity material in the Meissner state even though they exhibit similar behavior in the normal state. The normal-state behavior indicates that the effect of detuning the dislocation line is to decrease the energy absorbed from both the longitudinal and torsional modes. In the superconducting state the torsional-mode attenuation decreases with deformation while the longitudinal-mode increases. This may result from the differing coupling of the two acoustic modes to the underdamped motion of the dislocation in the Meissner state compared to the coupling to its overdamped motion in the normal state.

TABLE IX. Loss factor in the Meissner state for various imperfection densities; $T = 4.2$ °K.

Sample	Condition	Longitudinal η (10^{-6} Np)	Torsional η (10^{-6} Np)
No. 3 [111] RRR = 55	annealed	0.85	0.45
	quenched		1.16
	deformed		11.0
No. 5 [111] RRR = 2500	annealed	6.39	6.62
	quenched		6.60
	deformed		1.80
No. 4 [100] RRR = 2500	annealed	0.74	22.39
	quenched	1.72	
	deformed	2.45	

VI. ATTENUATION AS A FUNCTION OF FIELD

As the flux enters the bulk of the superconductor and the mixed state is established, the attenuation in the high-purity annealed material exhibits a rather unusual feature in the form of an initial decrease[33] with increasing magnetic field followed by an increase to a value in the normal state larger than the Meissner state [Fig. 2(a)]. The initial decrease has been observed previously in high-purity niobium and vanadium but not in lower-purity materials. One mechanism discussed previously interprets the decrease in attenuation as being due to the limitation of the Cooper-pair mean free path by the flux vortices.[34,35] The mechanism would predict a dependence of the attenuation on vortex density which is not observed in this investigation. In fact, the decrease in attenuation is observed to disappear for large imperfection densities even though the magnetic field dependence of the vortex density and electron mean free path remains substantially unchanged [Fig. 2(c)].

An alternate description of the attenuation decrease to that considered above is based on dislocation behavior, and is offered in the following. The length of segments of dislocations free to move in the high-purity niobium used in this investigation is greater than 10 μ. This length can be considerably less in materials of lower purity or those with a large imperfection density as one would obtain as a result of deformation. As discussed previously, the effective length of the vibrating dislocation line affects the acoustic energy absorbed through its influence on the matching of the acoustic-drive frequency to the resonance of

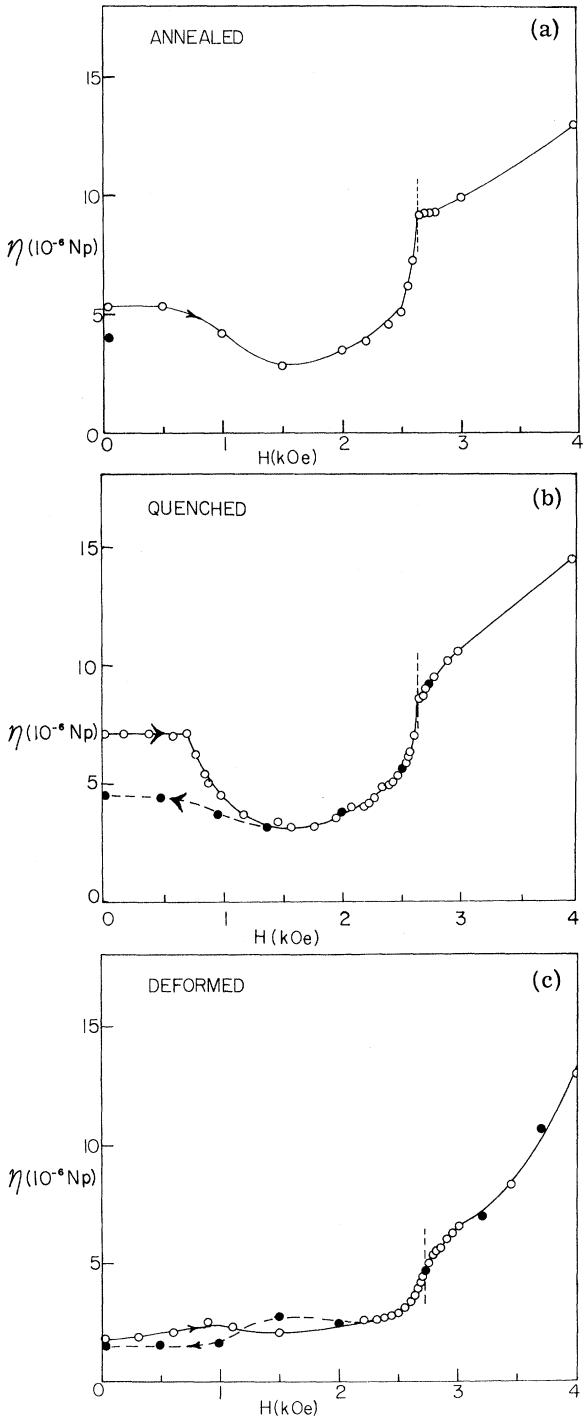

FIG. 2. Loss factor as a function of magnetic field for a torsional mode propagating along the [111] direction (No. 5) for various imperfection concentrations. As the imperfection concentration increases the attenuation in the Meissner state decreases due to the change in resonant-frequency distribution for the underdamped dislocation motion. The residual attenuation decreases with increasing imperfection concentration even though the number of trapped vortices increases slightly. The magnetic field is in the [110] direction.

the vibrating dislocation segment. A plausible model to explain the decrease in attenuation involves the variation of the matching of the dislocation motion to the acoustic wave through changes in its effective length and environment. When the magnetic field penetrates the superconductor it does so in the form of filaments of flux generated by a cylindrical vortex of supercurrent. The vortex has a core of normal material approximately one coherence length in diameter ($\xi_0 = 0.05\ \mu$ for high-purity niobium).[36] The presence of the vortices in the vicinity of the dislocation line can effectively change the length of the line by locally overdamping its motion. Since a typical length of the dislocation segment is 20 times the diameter of the vortex, the pinning would behave almost as a point constraint for low vortex densities. The decrease in effective length of the vibrating dislocation segment increases its resonance frequency making it even more remote from the frequency of the acoustic wave, therefore leading to poorer matching. The amount of energy absorbed by the dislocation system is reduced and thus its contribution to the attenuation of the acoustic wave is decreased. The attenuation then decreases as the mixed state is established due to the pinning of the dislocation motion by the vortex cores. The observed decrease in attenuation could result from a decrease in effective dislocation length of 15% according to the results of Granato and Lucke.[37] As the field is increased in the mixed state, the density of vortices increases and the isolated pinning of the dislocation motion no longer occurs since the vortices are of a higher density, cover much of the dislocation line, and interact strongly with each other. As the normal state is approached ($H \sim H_{c2}$) the damping due to the dislocation motion returns to its overdamped behavior and the attenuation increases rapidly to its normal-state value.

As supporting evidence that the behavior of the dislocations leads to the decrease in attenuation, the high-purity material is deformed to increase the dislocation density and decrease the length of the free segments. The decrease in attenuation for the torsional mode disappears and the magnitude of the attenuation decreases in the normal state. [Fig. 2(c)]. The latter effect is expected from the behavior predicted by the KGL theory for a decreased segment length, while the former results from the change in relative size of the dislocation segment and vortex size. As the dislocation segment length is decreased due to deformation, the size of the vortex becomes comparable and its impedence to the dislocation motion will not act at a point. The presence of the vortices are, therefore, much less effective in pinning the free dislocation segments and there is less change in matching conditions due to vortex penetration.

The attenuation of the torsional mode exhibits some unusual features in the immediate vicinity of H_{c2}. The magnitude of the change in attenuation between the superconducting and normal states is dominated by the change in dislocation damping from underdamped to overdamped due to the field-dependent contribution of the free electrons to the dislocation viscosity. The electronic contribution due to direct interaction with the perfect lattice[5] can be ignored at these low frequencies (< 5%). The superconducting transition affects the attenuation primarily by its contribution to the viscous damping of the dislocation motion. In the undeformed crystal the transition in attenuation at H_{c2} is well defined by a sharp change in slope from the rapidly increasing value in the intermediate state to the quadratic field dependence in the normal state (Fig. 3). As the imperfection concentration is increased the attenuation does not return to the normal-state value until significantly above H_{c2}. Determination of the second critical field is made simultaneously with the attenuation measurements by monitoring the behavior of the stiffness, thus including changes due to aging or deformation.

The diminished attenuation immediately above H_{c2} is shown to be dependent on the imperfection concentration in Fig. 3. The origin of the diminished attenuation may be due to the presence of transient Cooper pairs[38] whose lifetimes are finite above H_{c2}. The transient Cooper pairs serve to modify the transition of the dislocation motion from the underdamped superconducting state to the overdamped normal state. The attenuation is thus diminished immediately above H_{c2} but rapidly returns to the normal-state value as the lifetimes of the Cooper pairs decrease with increasing field. This is similar to observed behavior of the resistivity immediately above the surface superconducting transition in some superconductors.[39] The decrease in attenuation is more prominent in the deformed material which may be due to better matching between the resonance of the shortened dislocation line and the finite lifetimes of the Cooper pairs. A phenomenological model which includes resonant coupling leads to lifetimes of the order of 10^{-6} sec. This lifetime is longer than what might be expected from the temperature dependence of the transient pairing.

At fields appreciably above H_{c2} the attenuation exhibits the quadratic field dependence expected in the normal state. If a second-order polynomial is fitted to the observed values in the normal-state region, the attenuation obtained from extrapolating to zero field is less than that observed in the Meissner state. This suggests that if a normal state were possible at this temperature the attenuation would be less than in the superconducting state. Contributions of the dislocation motion to the attenuation are changed in both magnitude and frequency dependence when the motion is underdamped.

VII. COHERENCE PROPERTIES AND PHONON SCATTERING

Introduction of imperfections in high-purity niobium does not affect the low-temperature normal-state resistivity to within 10%. The normal-state electron mean free path remains relatively independent of the imperfection concentration. This is not true for the behavior of the second critical field which increases with increasing imperfection concentration. The origin of this change appears

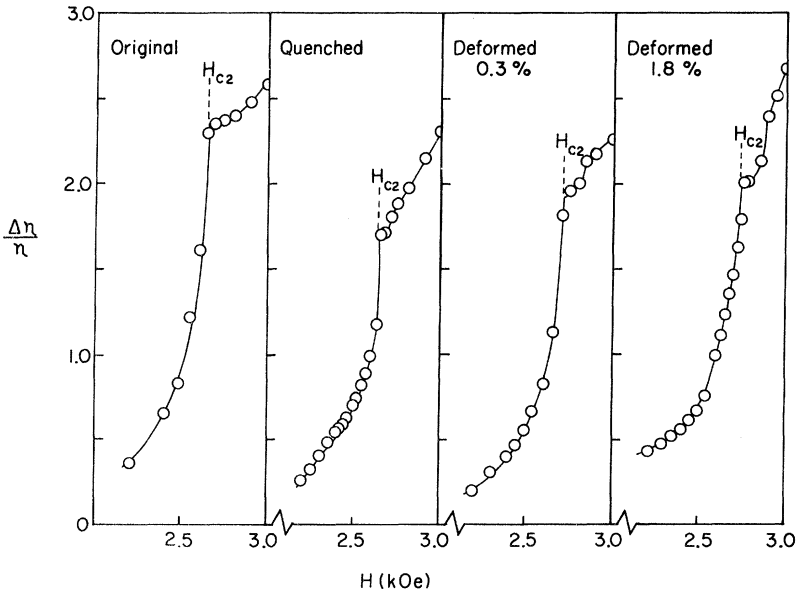

FIG. 3. Fractional change in attenuation of a torsional mode propagating along the [111] axis of specimen No. 5. The attenuation immediately above H_{c2} is less than the extrapolated normal-state value in the deformed material. The magnetic field is along the [110] direction; $T = 4.2$ °K.

TABLE X. Phonon-mean-free-path parameter calculated from Eqs. (7) and (8) and using $\xi_0 = 0.05\ \mu$; $T = 4.2$ °K. Sample No. 4.

Condition	H_{c2} (kOe)	$L(\mu)$
annealed	2.64	...
quenched	2.65	26.6
0.3% deformation	2.71	3.8
1.8% deformation	2.76	2.3

related to the reduction in phonon mean free paths by the imperfections and to the decrease in the correlation involved in forming the Cooper pairs. The effect is similar to limiting phonon mean free paths and thus pair lifetimes in nonisotropically pure materials.[40]

At magnetic fields near H_{c2} the Landau-Ginsburg equations can be linearized and a solution is obtained giving the second critical field[41] as

$$H_{c2} = \phi_0/2\pi\xi^2 \quad , \tag{6}$$

where ϕ_0 is the flux quanta (2×10^{-7} G cm^{-2}). This form provides order-of-magnitude agreement between the observed values for the coherence length and the second critical field. The coherence length exhibits an intrinsic limiting value in high-purity materials but decreases as the normal-state electron mean free path approaches the intrinsic coherence length (ξ_0). The impurities which limit the normal-state electron mean free path are not the only mechanisms which can limit the coherence properties of Cooper pairs but are often the dominant contribution. In addition, the coherence of the Cooper pairs can be limited by imperfections such as dislocations. In this investigation, H_{c2} for a fixed field direction is observed to increase with imperfection concentration. This behavior of H_{c2} suggests a modification of the coherence length analogous to that proposed by Pippard[5] to account for the limitation of the coherence properties due to the electron mean free path approaching the coherence length. This modification includes a term which is dependent on the phonon mean free path such that the reciprocal of the coherence length is given by

$$1/\xi = 1/\xi_0 + 1/l_e + 1/l_p \ , \tag{7}$$

where l_p is the term proportional to the phonon mean free path and l_e is the normal electron mean free path. For high-purity materials, such as sample Nos. 3 and 4 used in this investigation, the electron mean free path is much larger than the intrinsic coherence length ($l_e = 300\xi_0$) and the electronic contribution to the coherence length can be ignored. Assuming this additional contribution to the coherence length due to the finite phonon mean free path, the observed change in H_{c2} can be used to calculate l_p. The ratio of the second critical fields becomes

$$H_{c2}/H'_{c2} = \xi'^2/\xi_0^2 \quad , \tag{8}$$

where H_{c2} is for the annealed material with the least imperfection concentration and H'_{c2} and ξ' for material with an increased imperfection concentration.

Combining Eqs. (7) and (8) and using the observed values of H_{c2}, the parameter proportional to the phonon mean free path is calculated and displayed in Table X. Using these magnitudes to calculate the number of scatterings per unit volume leads to a number which is within an order of magnitude of the number of free dislocation segments expected in high-purity annealed material. The number of scatterings increases as the imperfection density increases, further suggesting the role played by dislocations in limiting the coherence of the Cooper pairs.

---

†Work supported by the National Science Foundation.

[1]J. L. Olsen, Nature 175, 37 (1955).

[2]G. A. Alers and D. L. Waldorf, Phys. Rev. Letters 6, 677 (1961); E. J. Kramer and C. L. Bauer, Phys. Rev. 163, 407 (1967).

[3]H. Bommel, Phys. Rev. 100, 758 (1955).

[4]J. N. Lange, J. Phys. Chem. Solids 31, 1693 (1970).

[5]A. B. Pippard, Proc. Roy. Soc. (London) A216, 547 (1953).

[6]J. Bardeen, L. N. Cooper, and J. R. Schrieffer, Phys. Rev. 108, 1175 (1957).

[7]B. R. Tittmann and H. E. Bommel, Phys. Rev. Letters 14, 296 (1965).

[8]W. P. Mason, in *Physical Acoustics*, edited by W. P. Mason (Academic, New York, 1966), Vol. 4A, Chap. 8.

[9]The loss factor (η) is defined as the energy absorbed per cycle to the energy stored per cycle times π. In terms of the attenuation coefficient α in Np/cm (1 Np = 8.68 dB), the group velocity v, and the radial frequency ω, the loss factor is given by $\eta = 2\alpha v/\omega$. The loss factor is related to the logarithmic decrement Λ as $\eta = \Lambda/\pi$.

[10]The fractional uncertainty in frequency (Δ) is given by $\Delta = (2\delta\eta^2)^{1/2}$, where δ is the fractional uncertainty in the resonance maximum.

[11]G. Goodrich and J. Lange, J. Acoust. Soc. Am. 50, 869 (1971).

[12]R. F. S. Hearman, Rev. Mod. Phys. 18, 409 (1946).

[13]High-purity specimens (Nos. 4 and 5), courtesy of R. E. Reed, Oak Ridge National Laboratory.

[14]R. E. Reed, H. D. Guberman, and T. O. Baldwin, J. Phys. Chem. Solids Suppl. 1, 829 (1967).

[15]G. A. Alers and P. A. Fleury, Phys. Rev. 129, 2425 (1963).

[16]J. N. Lange, Phys. Rev. 179, 631 (1969).

[17]J. S. Koehler, *Imperfections in Nearly Perfect Crystals* (Wiley, New York, 1952), p. 197.

[18]A. V. Granato and K. Lucke, J. Appl. Phys. 27, 583 (1956).
[19]H. Suhl, B. T. Matthias, and L. R. Walker, Phys. Rev. Letters 3, 552 (1959).
[20]I. M. Tang, Phys. Letters 31A, 480 (1970).
[21]J. R. Carlson and C. B. Satterthwaite, Phys. Rev. Letters 24, 461 (1970).
[22]L. J. Bruner and R. W. Keyes, Phys. Rev. Letters 7, 55 (1961).
[23]P. Csavinszky and N. G. Einspruch, Phys. Rev. 132, 2434 (1963).
[24]R. W. Keyes, IBM J. Res. Develop. 5, 266 (1961).
[25]E. Adler, IBM J. Res. Develop. 8, 430 (1964).
[26]V. Essmann and H. Trauble, Phys. Letters 24A, 526 (1967).
[27]G. W. Goodrich and J. N. Lange, Phys. Rev. 188, 728 (1969).
[28]C. Caroli, P. G. de Gennes, and J. Matricon, Phys. Letters 9, 309 (1964).
[29]P. de Gennes, *Superconductivity of Metals and Alloys* (Benjamin, New York, 1966), p. 65.
[30]W. Webb, Phys. Rev. Letters 11, 191 (1963).
[31]R. H. Chambers, in *Physical Acoustics*, edited by W. P. Mason (Academic, New York, 1966), Vol. 2A, Chap. 4.
[32]E. J. Kramer and C. L. Bauer, Phil. Mag. 15, 1189 (1967).
[33]E. M. Forgan and C. E. Gough, Phys. Letters 21, 133 (1966).
[34]A. C. E. Sinclair and J. R. Leibowitz, Phys. Rev. 175, 596 (1968).
[35]R. M. Cleary, Phys. Rev. 175, 587 (1968).
[36]D. K. Finnemore, T. F. Stromberg, and C. A. Swenson, Phys. Rev. 149, 231 (1966).
[37]A. Granato and K. Lucke, in *Physical Acoustics*, edited by W. P. Mason (Academic, New York, 1966), Vol. 4A, Chap. 6.
[38]R. A. Ferrell and H. Schmidt, Phys. Letters 25A, 544 (1967); H. Schmidt, Z. Physik 216, 336 (1968).
[39]R. R. Hake, Phys. Rev. Letters 23, 1105 (1969).
[40]R. E. Fassnacht and J. R. Dillinger, Phys. Rev. Letters 24, 1059 (1970).
[41]P. de Gennes, *Superconductivity of Metals and Alloys* (Benjamin, New York, 1966), p. 196.